Received December 17, 2017, accepted February 19, 2018, date of publication April 16, 2018, date of current version June 29, 2018.

Digital Object Identifier 10.1109/ACCESS.2018.2820089

Analysis of Two Dimensional Graphene-Based Multilayered Structures Using the Extended Method of Lines

ALI MEHRDADIAN, HOSSEIN HATEFI ARDAKANI, AND KEYVAN FOROORAGHI
Department of Electrical and Computer Engineering, Tarbiat Modares University, Tehran 14115, Iran
Corresponding authors: Ali Mehrdadian (ali.mehrdadian@modares.ac.ir) and Keyvan Forooraghi (keyvan_f@modares.ac.ir)

ABSTRACT In this paper, the method of lines is extended to analyze 2-D graphene-based multilayered structures. The graphene plates with tensor conductivity may cover partially or totally the interfaces between two consecutive layers. In this paper, the impedance and admittance transformations through the graphene-contained interfaces are developed. Also, the characteristic equation of the graphene-contained multilayered structure is obtained by matching the tangential fields at the graphene sheet. To verify the obtained relations, the following structures are analyzed using the extended method of lines: graphene-based microstrip lines, graphene-based striplines, and graphene-based parallel-plate waveguides. The results of the analysis of the graphene-based microstrip line are compared with the results obtained from the spectral domain approach and COMSOL software, whereas the results of the analysis of the graphene-based stripline and parallel-plate waveguide are compared with those of COMSOL software, which show a good agreement. The conductivity of graphene can be adjusted by varying parameters such as the bias of electric and magnetic fields perpendicular to the graphene sheet. Also, a parametric study is carried out on these parameters by which the characteristics of the analyzed structures can be controlled. The tunable structures are vastly used in new microwave applications.

INDEX TERMS Graphene, extended method of lines (E-MOL), impedance and admittance transformation, multilayered structures, spectral domain method (SDM), microstrip, stripline, parallel-plate waveguide.

I. INTRODUCTION

Graphene, a two dimensional arrangement of carbon atoms in a hexagonal lattice, is a promising material in the field of electronics and electromagnetics and have attracted enormous attention in the recent years [1], [2]. Although the theory of graphene was first explored in 1948, the first sheets of graphene with dimensions of around a few micrometers were made in 2004. The graphene sheets encompass electrical properties such as tunability of conductivity with a biased voltage which make it suitable for the electronic devices with the ability of controlling their characteristics [3]. New devices with the dimensions of nanometer scale such as antennas, flexible electronic devices, touch screens and ultrahigh speed transistors are some of the applications of the graphene sheets [4]–[6]. Nowadays, the graphene sheets with dimensions of about 30cm are being produced, so that their application in the fields of microwave and millimeter wave have received remarkable interest [4], [7]. The linear and gapless electronic band structure arising from its particular atomic structure, have made graphene possess unique and exclusive properties. Particularly, the linear momentum-energy dispersion, analogous to the dispersion of photons in free space, causes the electrons to act as massless particles. Therefore, graphene may exhibit a mobility of 500000 cm2/Vs. These properties have made graphene the subject of great attention in high speed electronic devices [8], [9].

Kubo [9] presented the most accurate model of graphene conductivity which includes all parameters affecting the conductivity:

$$\overline{\overline{\sigma}} = \sigma_d \left(\hat{x}\hat{x} + \hat{z}\hat{z}\right) + \sigma_o \left(\hat{z}\hat{x} - \hat{x}\hat{z}\right) \tag{1}$$

where

$$\sigma_d \left(\mu_c \left(E_0\right), B_0\right) = \frac{e^2 v_F^2 \left|eB_0\right| \left(\omega - j2\Gamma\right)\hbar}{-j\pi} \times \sum_{n=0}^{\infty} \left\{ \frac{f_d\left(M_n\right) - f_d\left(M_{n+1}\right) + f_d\left(-M_{n+1}\right) - f_d\left(-M_n\right)}{\left(M_{n+1} - M_n\right)^2 - \left(\omega - j2\Gamma\right)^2 \hbar^2} \times \left(1 - \frac{\Delta^2}{M_n M_{n+1}}\right) \frac{1}{M_{n+1} - M_n}$$

$$+\frac{f_d(-M_n)-f_d(M_{n+1})+f_d(-M_{n+1})-f_d(-M_n)}{(M_{n+1}+M_n)^2-(\omega-j2\Gamma)^2\hbar^2}\times\left(1+\frac{\Delta^2}{M_nM_{n+1}}\right)\frac{1}{M_{n+1}+M_n}\Bigg\} \quad (2)$$

and

$$\sigma_o(\mu_c(E_0),B_0)=\frac{e^2v_F^2eB_0}{\pi}\times\sum_{n=0}^{\infty}\{f_d(M_n)-f_d(M_{n+1})+f_d(-M_{n+1})-f_d(-M_n)\}\left\{\frac{1}{(M_{n+1}-M_n)^2-(\omega-j2\Gamma)^2\hbar^2}\times\left(1-\frac{\Delta^2}{M_nM_{n+1}}\right)+\frac{1}{(M_{n+1}-M_n)^2-(\omega-j2\Gamma)^2\hbar^2}\times\left(1+\frac{\Delta^2}{M_nM_{n+1}}\right)\right\} \quad (3)$$

with

$$M_n=\sqrt{\Delta^2+2nv_F^2|eB_0|\hbar} \quad (4)$$

where μ_c is the chemical potential (which can be controlled by applied electrostatic bias field $E_0=\hat{z}E_0$, or by doping), Γ is the phenomenological electron scattering rate that is assumed to be independent of energy, $B_0=\hat{z}B_0$ is the applied magnetostatic bias field, e is the charge density of an electron, $\hbar=h/2\pi$ is the reduced Planck's constant, $v_F=10^6m/s$ is the electron's energy-independent velocity, Δ is an excitonic energy gap, $f_d(\varepsilon)=(e^{(\varepsilon-\mu_c)/K_BT}+1)^{-1}$ is the Fermi-Dirac distribution, which ε is energy and K_B is Boltzmann's constant.

Various methods have been utilized to analyze the graphene-contained structures, each having its advantages and disadvantages. The fully analytical approaches suffer restrictions regarding their use in complex structures since a limited number of structures can be analyzed analytically [10]–[15]. Fully numerical methods can be used to analyze complex structures, however because of their fully numerical nature, the simulation time may be too long [16], [2], and [1]. Therefore, a method is required which is capable of simultaneous numerical and analytical analysis where the simulation time is reduced due to the fact that a part of the problem is solved analytically.

Regarding the two-dimensional structure of the graphene, the graphene-contained structures can be modeled by a multilayered structure. The method of lines is a semi-numerical semi-analytical method. Since a part of the problem is analyzed analytically, the method of lines requires less simulation time than the fully numerical methods [17]. This method is considerably useful to analyze the multilayered structures or the structures that can be divided into several layers with reasonable approximation [18]. Method of lines was first used to analyze the semi-plate waveguide structures. It can also be used to analyze the two-dimensional and three-dimensional structures which require one-dimensional and two-dimensional discretizations, respectively [19], [20].

In the present paper, the multilayered two-dimensional structures with arbitrary number of layers including graphene sheets between the layers, is analyzed using the extended method of lines. To this end, the formula for the admittance transformation through a graphene sheet is developed. From which, the impedance and admittance transformation of the entire multilayered structure containing graphene sheets can be performed. In order to verify the method in the case of multilayered structures, three example structures are analyzed. First, a graphene-based microstrip line is investigated and its characteristic equation in the extended method of lines is developed using the field matching at the graphene-contained plate. By varying the chemical potential of the graphene, the characteristics of the microstrip line can be modified. The method is verified by comparing the results of the analysis with those obtained from the spectral domain approach and COMSOL software. The second structure analyzed here is a graphene-based stripline. The results of this structure are also compared with the results of COMSOL software. Finally, the third structure is a graphene-based parallel-plate waveguide, the results of which are compared with those of COMSOL software. The comparison of the results demonstrates the reliability of the extended method of lines to analyze the multilayered structures. These examples are meant to verify the proposed method, whereas this method is general and is able to analyze a variety of two-dimensional multilayered structures in rectangular, cylindrical, and spherical coordinate systems. In the following and in section II, the numerical methods are presented to analyze multilayered graphene-based structures. First, the extended method of lines is presented to analyze general two-dimensional graphene-based multilayered structures. Second, the spectral domain method is explained to analyze the graphene-based microstrip line. In section III, the calculation details with the COMSOL software is presented. In section IV, the results obtained from the analysis of three aforesaid structures using the proposed method are compared with those of COMSOL software. Finally, in section V the conclusions are provided.

II. NUMERICAL METHODS

The method of lines can be used to analyze the multilayered structures. Impedance and admittance transformation through various layers and also impedance and admittance transformation through the interfaces are crucial in the method of lines. In the following, first the application of the method of lines in the analysis of the multilayered structures is described, and then the equations of the impedance and admittance transformation through the graphene-contained interface of two layers are obtained. In the method of lines, by the impedance and admittance transformation from the two sides of the structure and matching the fields within a plane, the multilayered characteristic equation is obtained. Also, in the following the characteristic equation of the graphene-contained multilayered structure is obtained by matching the tangential fields at the graphene sheet. As an example of multilayered structures, the characteristic equation of

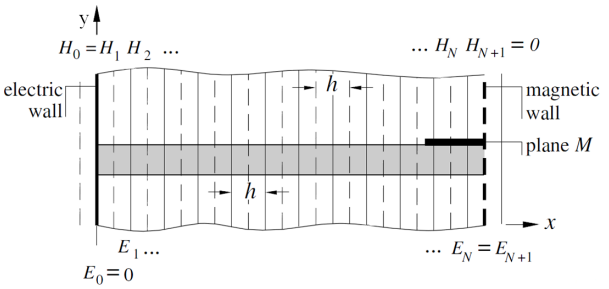

FIGURE 1. Cross section of a planar waveguide with discretized lines, Solid lines: The electric field lines, Dashed lines: The magnetic field lines.

a graphene-based microstrip line is presented. At the end of this section, the analysis of graphene-based microstrip line using the spectral domain method is also presented.

A. METHOD OF LINES IN THE ANALYSIS OF THE MULTILAYERED STRUCTURES

The electromagnetic fields in the planar waveguide structures, which are used in optical or microwave integrated circuits, can be obtained from two independent field components or two independent potential components. The components e_z and h_z must satisfy the Helmholtz equation within each layer [17]:

$$\frac{\partial^2\psi}{\partial x^2}+\frac{\partial^2\psi}{\partial y^2}+\frac{\partial^2\psi}{\partial z^2}+k^2\psi = L\psi = 0 \tag{5}$$

$$k^2 = \varepsilon_r k_0^2 \quad k_0 = \omega\sqrt{\mu_0\varepsilon_0} \tag{6}$$

where ψ represents each of the components e_z and h_z. The microstrip line illustrated in Fig. 1 is considered as an example. Assume that the number of discretized lines for the e_z and h_z fields in Fig. 1 is equal to N. The fields e_z and h_z on the discretized lines are collected in $\mathbf{E}_z$ and $\mathbf{H}_z$ vectors. The i'th component of the $\mathbf{E}_z$ vector indicates the electric field e_z on the i'th line. It should also be noted that E_{zi} is a function of y. In order to discretize (5), the derivative with respect to x must be replaced by an appropriate fraction. We have [21]:

$$h\frac{\partial e_z}{\partial x} \rightarrow \boldsymbol{D}\mathbf{E}_z \tag{7}$$

$$h\frac{\partial h_z}{\partial x} \rightarrow -\boldsymbol{D}^t\mathbf{H}_z \tag{8}$$

Equation (8) shows that the difference operator $\boldsymbol{D}$ which is used to take the derivative of e_z can also be used to take the derivative of h_z. The difference operator $\boldsymbol{D}$ has a form that satisfies the lateral boundary conditions. Also the second derivative of the fields can be defined as [22]:

$$h^2\frac{\partial^2 e_z}{\partial x^2} \rightarrow -\boldsymbol{D}^t\boldsymbol{D}\mathbf{E}_z = -\boldsymbol{P}_{DN}\mathbf{E}_z \tag{9}$$

$$h^2\frac{\partial^2 h_z}{\partial x^2} \rightarrow -\boldsymbol{D}\boldsymbol{D}^t\mathbf{E}_z = -\boldsymbol{P}_{ND}\mathbf{E}_z \tag{10}$$

By substituting (9) or (10) into (5), the following ordinary differential equation is obtained:

$$\frac{d^2}{dy^2}\psi+\left[\left(k^2-k_z^2\right)\boldsymbol{I}-h^{-2}\boldsymbol{P}\right]\psi = \mathbf{0} \tag{11}$$

The convention for the wave propagation in the z direction is considered as $e^{-jk_z z}$, ψ represents the vectors $\mathbf{E}_z$ or $\mathbf{H}_z$, and $\boldsymbol{P}$ is their corresponding difference matrix. In this equation $\boldsymbol{I}$ is the unity matrix. Since $\boldsymbol{P}$ is a tridiagonal matrix, in (11) three components of ψ vector are always dependent to each other, and consequently these equations can't be solved directly. To solve this problem a transformation is carried out [17]:

$$\psi = \boldsymbol{T}\bar{\boldsymbol{\psi}} \tag{12}$$

requiring that:

$$\boldsymbol{T}^t\mathbf{P}\mathbf{T} = \lambda^2 \tag{13}$$

The matrices λ^2 and $\boldsymbol{T}$ are the diagonal eigenvalue matrix and eigenvector matrix of $\boldsymbol{P}$, respectively. For different BCs determining the $\boldsymbol{P}$ matrix, the matrices λ^2 and $\boldsymbol{T}$ are calculated analytically. Since the matrix $\boldsymbol{P}$ is symmetric, with a suitable normalization of the eigenvectors, the $\boldsymbol{T}$ matrix reduces to an orthogonal matrix:

$$\boldsymbol{T}^{-1} = \boldsymbol{T}^t \tag{14}$$

By substituting (12) and (13) into (11) [17]:

$$\left[\left(\frac{d^2}{dy^2}+k^2-k_z^2\right)\mathrm{I}-h^{-2}\lambda^2\right]\bar{\boldsymbol{\psi}} = \mathbf{0} \tag{15}$$

Let

$$k_{yi}^2 = k_0^2\left(\bar{\lambda}_i^2-\varepsilon_r+\varepsilon_{re}\right)$$

$$\varepsilon_{re} = \frac{k_z^2}{k_0^2}, \bar{\lambda}_i^2 = \frac{\lambda_i^2}{(k_0 h)^2} \tag{16}$$

Hence the general solution for the i'th component of $\bar{\boldsymbol{\psi}}$ vector can be written as:

$$\bar{\boldsymbol{\psi}}_i = A_i\cosh k_{yi}y + B_i\sinh k_{yi}y \tag{17}$$

In the method of lines, in most cases the field components and their derivatives at the interface between the layers are required. Using (17) the relation between the field components and their derivatives in a layer with the thickness d, shown in Fig. 2, can be obtained as [17]:

$$\begin{bmatrix}\bar{\boldsymbol{\psi}}'(y_1)\\ \bar{\boldsymbol{\psi}}'(y_2)\end{bmatrix} = \boldsymbol{k}_y^2\begin{bmatrix}\boldsymbol{\gamma} & \boldsymbol{\alpha}\\ \boldsymbol{\alpha} & \boldsymbol{\gamma}\end{bmatrix}\begin{bmatrix}-\bar{\boldsymbol{\psi}}(y_1)\\ \bar{\boldsymbol{\psi}}(y_2)\end{bmatrix} \tag{18}$$

where

$$\bar{\boldsymbol{\psi}}' = \frac{1}{k_0}\frac{d}{dy}\bar{\boldsymbol{\psi}} \tag{19}$$

$$\boldsymbol{\alpha} = \mathrm{diag}\left(\frac{k_{yi}}{k_0}sinh\, k_{yi}d\right)^{-1} \tag{20}$$

$$\boldsymbol{\gamma} = \mathrm{diag}\left(\frac{k_{yi}}{k_0}tanh\, k_{yi}d\right)^{-1} \tag{21}$$

$$\boldsymbol{k}_y = \mathrm{diag}\left(\frac{k_{yi}}{k_0}\right) \tag{22}$$

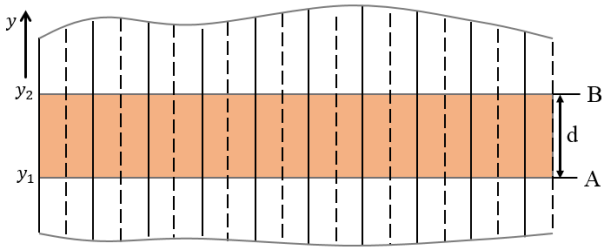

FIGURE 2. Cross section of a multilayered structure.

Using the Maxwell equations, the transformed field components are calculated from the independent components $\bar{\mathbf{E}}_z$ and $\bar{\mathbf{H}}_z$ as:

$$\varepsilon_d \begin{bmatrix} \bar{\mathbf{E}}_x \\ \eta_0 \bar{\mathbf{H}}_x \end{bmatrix} = \mathrm{j} \begin{bmatrix} -\sqrt{\varepsilon}_{re}\bar{\boldsymbol{\delta}} & -\boldsymbol{I}\dfrac{1}{k_0}\dfrac{\partial}{\partial y} \\ \boldsymbol{I}\dfrac{\varepsilon_r}{k_0}\dfrac{\partial}{\partial y} & \sqrt{\varepsilon}_{re}\bar{\boldsymbol{\delta}}^{\mathrm{t}} \end{bmatrix} \begin{bmatrix} \bar{\mathbf{E}}_z \\ \eta_0 \bar{\mathbf{H}}_z \end{bmatrix} \quad (23)$$

$$\varepsilon_d \begin{bmatrix} \bar{\mathbf{E}}_y \\ \eta_0 \bar{\mathbf{H}}_y \end{bmatrix} = -\mathrm{j} \begin{bmatrix} \boldsymbol{I}\dfrac{\sqrt{\varepsilon}_{re}}{k_0}\dfrac{\partial}{\partial y} & \bar{\boldsymbol{\delta}}^{\mathrm{t}} \\ \varepsilon_r\bar{\boldsymbol{\delta}} & \boldsymbol{I}\dfrac{\sqrt{\varepsilon}_{re}}{k_0}\dfrac{\partial}{\partial y} \end{bmatrix} \begin{bmatrix} \bar{\mathbf{E}}_z \\ \eta_0 \bar{\mathbf{H}}_z \end{bmatrix} \quad (24)$$

where

$$\bar{\boldsymbol{\delta}} = (k_0 h)^{-1}\boldsymbol{\delta}, \boldsymbol{\delta} = \boldsymbol{T}_h^t \boldsymbol{D} \boldsymbol{T}_e, \quad \varepsilon_d = \varepsilon_r - \varepsilon_{re} \quad (25)$$

The matrix δ is a diagonal or quasi-diagonal matrix. In the above equation, $\boldsymbol{T}_e$ is the transformation matrix for $\mathbf{E}_z$, and $\boldsymbol{T}_h$ is the transformation matrix for $\mathbf{H}_z$. The system of equations (23) and (24) is written for the interface plates A and B, represented in Fig. 2. Hence from (18) and this system of equations, we have [17]:

$$\eta_0 \begin{bmatrix} -j\bar{\mathbf{H}}_{zA} \\ \bar{\mathbf{H}}_{xA} \\ -j\bar{\mathbf{H}}_{zB} \\ \bar{\mathbf{H}}_{xB} \end{bmatrix} = \begin{bmatrix} -\varepsilon_d\boldsymbol{\gamma}_h & \boldsymbol{\gamma}_h\tilde{\boldsymbol{\delta}} & -\varepsilon_d\boldsymbol{\alpha}_h & \boldsymbol{\alpha}_h\tilde{\boldsymbol{\delta}} \\ \tilde{\boldsymbol{\delta}}^t\boldsymbol{\gamma}_h & \boldsymbol{\gamma}_E & \tilde{\boldsymbol{\delta}}^t\boldsymbol{\alpha}_h & \boldsymbol{\alpha}_E \\ -\varepsilon_d\boldsymbol{\alpha}_h & \boldsymbol{\alpha}_h\tilde{\boldsymbol{\delta}} & -\varepsilon_d\boldsymbol{\gamma}_h & \boldsymbol{\gamma}_h\tilde{\boldsymbol{\delta}} \\ \tilde{\boldsymbol{\delta}}^t\boldsymbol{\alpha}_h & \boldsymbol{\alpha}_E & \tilde{\boldsymbol{\delta}}^t\boldsymbol{\gamma}_h & \boldsymbol{\gamma}_E \end{bmatrix} \begin{bmatrix} \bar{\mathbf{E}}_{xA} \\ -j\bar{\mathbf{E}}_{zA} \\ -\bar{\mathbf{E}}_{xB} \\ j\bar{\mathbf{E}}_{zB} \end{bmatrix} \quad (26)$$

where

$$\tilde{\boldsymbol{\delta}} = \sqrt{\varepsilon}_{re}\bar{\boldsymbol{\delta}}, \boldsymbol{\alpha}_E = \varepsilon_d^{-1}\left[\varepsilon_r \boldsymbol{k}_{ye}^2\boldsymbol{\gamma}_e - \tilde{\boldsymbol{\delta}}^t\boldsymbol{\gamma}_h\tilde{\boldsymbol{\delta}}\right],$$
$$\boldsymbol{\gamma}_E = \varepsilon_d^{-1}\left[\varepsilon_r \boldsymbol{k}_{ye}^2\boldsymbol{\alpha}_e - \tilde{\boldsymbol{\delta}}^t\boldsymbol{\gamma}_h\tilde{\boldsymbol{\delta}}\right] \quad (27)$$

In the above equations the subscripts e or h are used for the parameters $\boldsymbol{\alpha}$, $\boldsymbol{\gamma}$ and $\boldsymbol{\lambda}$ considering that ψ represents each of e_z or h_z. Using the abbreviations:

$$\bar{\mathbf{H}}_{A,B} = \eta_0 \begin{bmatrix} -\mathrm{j}\bar{\mathbf{H}}_{zA,B} \\ \bar{\mathbf{H}}_{xA,B} \end{bmatrix}, \quad \bar{\mathbf{E}}_{A,B} = \begin{bmatrix} \bar{\mathbf{E}}_{xA,B} \\ -\mathrm{j}\bar{\mathbf{E}}_{zA,B} \end{bmatrix} \quad (28)$$

and also

$$\bar{\mathbf{y}}_1 = \begin{bmatrix} -\varepsilon_d\boldsymbol{\gamma}_h & \boldsymbol{\gamma}_h\tilde{\boldsymbol{\delta}} \\ \tilde{\boldsymbol{\delta}}^t\boldsymbol{\gamma}_h & \boldsymbol{\gamma}_E \end{bmatrix} \quad \bar{\mathbf{y}}_2 = \begin{bmatrix} -\varepsilon_d\boldsymbol{\alpha}_h & \boldsymbol{\alpha}_h\tilde{\boldsymbol{\delta}} \\ \tilde{\boldsymbol{\delta}}^t\boldsymbol{\alpha}_h & \boldsymbol{\alpha}_E \end{bmatrix} \quad (29)$$

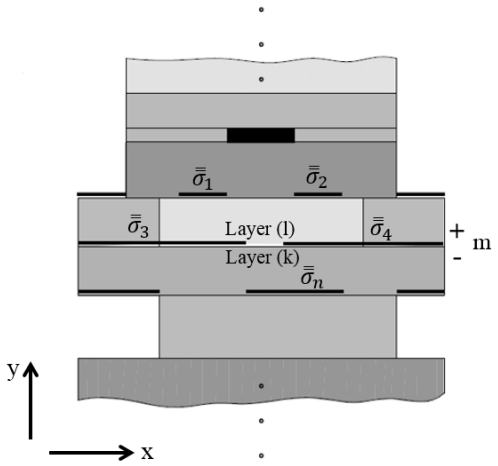

FIGURE 3. Multilayered structure and graphene-contained interfaces.

the equation (26) is reduced to the simple form:

$$\begin{bmatrix} \bar{\mathbf{H}}_A \\ \bar{\mathbf{H}}_B \end{bmatrix} = \begin{bmatrix} \bar{\mathbf{y}}_1 & \bar{\mathbf{y}}_2 \\ \bar{\mathbf{y}}_2 & \bar{\mathbf{y}}_1 \end{bmatrix} \begin{bmatrix} \bar{\mathbf{E}}_A \\ -\bar{\mathbf{E}}_B \end{bmatrix} \quad (30)$$

Assuming an electric wall at the 0'th interface, the tangential electric field on that interface is zero $(\bar{\mathbf{E}}_0 = 0)$, so from (30) for the first layer in the first step we have:

$$\bar{\mathbf{H}}_1 = \bar{\mathbf{Y}}_{\mathrm{t}}^{(1)}\bar{\mathbf{E}}_1 \quad (31)$$

where

$$\bar{\mathbf{Y}}_{\mathrm{t}}^{(1)} = -\bar{\mathbf{y}}_1 \quad (32)$$

The parameter $\bar{\mathbf{y}}_1$ is calculated using the properties of the 1'st layer. In the same way, using (30), the impedance and admittance transformation equation between the two plates of a layer can be obtained.

To utilize the method of lines in the graphene-based multilayered structures, the impedance and admittance transformation equations through the graphene-contained interface will be derived in the next section.

B. IMPEDANCE AND ADMITTANCE TRANSFORMATION THROUGH A GRAPHENE CONTAINED INTERFACE

As shown in Fig. 3, the interfaces are numbered and the fictitious planes just above and below an interface are indicated by + and − signs, respectively.

As shown in Fig. 3, the graphene plates are placed on the zx plane. In the method of lines, the equations are solved analytically in the y direction so the impedance and admittance transformation is performed in the y direction. A graphene-contained interface is numbered m. Then, the relation between the admittance above $\left(\bar{\mathbf{Y}}_{t^-}^{(m)}\right)$ and below $\left(\bar{\mathbf{Y}}_{t^+}^{(m)}\right)$ the interface must be obtained. The current density in the graphene plate is calculated as:

$$\begin{bmatrix} \mathrm{J}_x \\ \mathrm{J}_x \end{bmatrix} = \begin{bmatrix} \sigma_{xx}E_x + \sigma_{zx}E_z \\ -\sigma_{zx}E_x + \sigma_{xx}E_z \end{bmatrix} = \begin{bmatrix} \sigma_{xx} & \sigma_{zx} \\ -\sigma_{zx} & \sigma_{xx} \end{bmatrix} \begin{bmatrix} E_x \\ E_z \end{bmatrix}$$
$$= \bar{\bar{\sigma}}. \begin{bmatrix} E_x \\ E_z \end{bmatrix} \quad (33)$$

The transverse electric fields at the m'th interface are continuous, so we have:

$$\begin{bmatrix} E_x \\ E_z \end{bmatrix}^{m^+} = \begin{bmatrix} E_x \\ E_z \end{bmatrix}^{m^-} = \begin{bmatrix} E_x \\ E_z \end{bmatrix}^{m} = \vec{E}_m \tag{34}$$

The boundary condition for the magnetic field at the interface between each two layers is:

$$\hat{n} \times \left(\vec{H}_2 - \vec{H}_1\right) = \vec{J}_s \tag{35}$$

where at the m'th interface, it takes the form:

$$\hat{n} \times \left(\vec{H}_{m^+} - \vec{H}_{m^-}\right) = \vec{J}_m = \overline{\overline{\sigma}}.\vec{E}_m \tag{36}$$

By the substitution of:

$$\vec{H}_{m^+} = H_{xm^+}\hat{x} + H_{zm^+}\hat{z} \tag{37}$$
$$\vec{H}_{m^-} = H_{xm^-}\hat{x} + H_{zm^-}\hat{z} \tag{38}$$

in (36) and assuming that $\hat{n} = \hat{y}$, we have:

$$\begin{aligned} \hat{y} \times \left(H_{xm^+}\hat{x} + H_{zm^+}\hat{z} - H_{xm^-}\hat{x} - H_{zm^-}\hat{z}\right) &= \overline{\overline{\sigma}}.\vec{E}_m \\ - H_{xm^+}\hat{z} + H_{zm^+}\hat{z} + H_{xm^-}\hat{z} - H_{zm^-}\hat{z} & \\ = \left(\sigma_{xx}E_{xm} + \sigma_{zx}E_{zm}\right)\hat{x} + \left(-\sigma_{zx}E_{xm} + \sigma_{xx}E_{zm}\right)\hat{z} & \end{aligned} \tag{39}$$

By separating this equation into $\hat{x}$ and $\hat{z}$ components, we have:

$$H_{zm^+} = H_{zm^-} + \sigma_{xx}E_{xm} + \sigma_{zx}E_{zm} \tag{40}$$
$$H_{xm^+} = H_{xm^-} + \sigma_{zx}E_{xm} - \sigma_{xx}E_{zm} \tag{41}$$

The electric and magnetic fields vectors are defined as:

$$E = \begin{bmatrix} E_x \\ -jE_z \end{bmatrix} H = \eta_0 \begin{bmatrix} -jH_z \\ H_x \end{bmatrix} \tag{42}$$

Accordingly, (40) and (41) can be rewritten as:

$$\begin{aligned} \eta_0 \begin{bmatrix} -jH_{zm^+} \\ H_{xm^+} \end{bmatrix} &= \eta_0 \begin{bmatrix} -jH_{zm^-} \\ H_{xm^-} \end{bmatrix} \\ &+ \eta_0 \begin{bmatrix} -j\sigma_{xx} & \sigma_{zx} \\ \sigma_{zx} & -j\sigma_{xx} \end{bmatrix} \begin{bmatrix} E_{xm} \\ -jE_{zm} \end{bmatrix} \end{aligned} \tag{43}$$

$$H_{m^+} = H_{m^-} + \begin{bmatrix} -j\eta_0\sigma_{xx} & \eta_0\sigma_{zx} \\ \eta_0\sigma_{zx} & -j\eta_0\sigma_{xx} \end{bmatrix} E_m \tag{44}$$

In the method of lines, impedance and admittance transformation is performed in the transformed domain. Therefore, (44) must be written in the transformed domain and subsequently, using the fields relations in the transformed domain, the impedance and admittance transformation is performed. It is assumed here that discretization is done in one direction. The fields discretization positions and parameters of graphene for a microstrip line are illustrated in Fig. 4. It should be noted that each parameter σ_{xx} and σ_{zx} must be discretized in two different positions: the solid lines and the dashed lines. The conductivity σ_{xxh} indicates the value of σ_{xx} on the dashed lines, and σ_{xxe} indicates the value of σ_{xx} on the solid lines. In the same way, σ_{zx} is indicated by the two terms σ_{zxh} and σ_{zxe}. The conductivity σ_{zxh} shows the value of σ_{zx} on

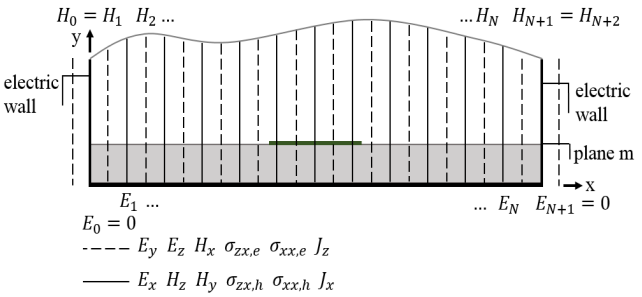

FIGURE 4. Graphene-based microstrip line and the discretization lines.

the dashed lines, and σ_{zxe} shows the value of σ_{zx} on the solid lines. Then, (40) and (41) are rewritten as:

$$\begin{aligned} -j\eta_0\mathbf{H}_{zm^+} &= -j\eta_0\mathbf{H}_{zm^-} - j\eta_0\boldsymbol{\sigma}_{xxh}\mathbf{E}_{xm} \\ &+ \eta_0\boldsymbol{\sigma}_{zxe}\left(-j\mathbf{E}_{zm}\right) \end{aligned} \tag{45}$$

$$\begin{aligned} \eta_0\mathbf{H}_{xm^+} &= \eta_0\mathbf{H}_{xm^-} + \eta_0\boldsymbol{\sigma}_{zxh}\mathbf{E}_{xm} \\ &- j\eta_0\boldsymbol{\sigma}_{xxe}\left(-j\mathbf{E}_{zm}\right) \end{aligned} \tag{46}$$

Another point that should be noted is that the position of the fields components are different from each other, for instance in (45) the component E_x is discretized at different positions than those of E_z and H_x components, and Hence the term $\boldsymbol{\sigma}_{zxh}\mathbf{E}_{xm}$ cannot be added or subtracted from them directly. Also, in (46) the E_z component is discretized at different positions than those of E_x and H_z components, and consequently the term $\boldsymbol{\sigma}_{zxe}\left(-j\mathbf{E}_{zm}\right)$ cannot be added or subtracted from them directly. To overcome this problem, the interpolation matrices should be utilized to obtain the values of $\boldsymbol{\sigma}_{zxh}\mathbf{E}_{xm}$ and $\boldsymbol{\sigma}_{zxe}\left(-j\mathbf{E}_{zm}\right)$ at the correct positions. Accordingly, (45) and (46) are rewritten as:

$$-j\eta_0\mathbf{H}_{zm^+} = -j\eta_0\mathbf{H}_{zm^-} - j\eta_0\boldsymbol{\sigma}_{xxh}\mathbf{E}_{xm} + \eta_0\boldsymbol{M}_x^e\boldsymbol{\sigma}_{zxe}\left(-j\mathbf{E}_{zm}\right) \tag{47}$$

$$\begin{aligned} \eta_0\mathbf{H}_{xm^+} &= \eta_0\mathbf{H}_{xm^-} + \eta_0\boldsymbol{M}_x^h\boldsymbol{\sigma}_{zxh}\mathbf{E}_{xm} \\ &- j\eta_0\boldsymbol{\sigma}_{xxe}\left(-j\mathbf{E}_{zm}\right) \end{aligned} \tag{48}$$

As the impedance and admittance transformation is performed in the transformed domain, the fields components in the transformed domain are obtained by their multiplication with suitable transformation matrices according to their discretization position. Here we assume that the widths of the two layers at both sides of the m'th interface are equal, and also the boundary conditions for the two layers are the same. As seen in Fig. 4, the components that are placed on the lines are transformed by the matrix $\boldsymbol{T}_e$, and the components which are placed on the dashed lines are transformed by the matrix $\boldsymbol{T}_h$. As a result, in the transformed domain (47) and (48) are written as:

$$\begin{aligned} -j\eta_0\boldsymbol{T}_h\bar{\mathbf{H}}_{zm^+} &= -j\eta_0\boldsymbol{T}_h\bar{\mathbf{H}}_{zm^-} - j\eta_0\boldsymbol{\sigma}_{xxh}\boldsymbol{T}_h\bar{\mathbf{E}}_{xm} \\ &+ \eta_0\boldsymbol{M}_x^e\boldsymbol{\sigma}_{zxe}\boldsymbol{T}_e\left(-j\bar{\mathbf{E}}_{zm}\right) \end{aligned} \tag{49}$$

$$\begin{aligned} \eta_0\boldsymbol{T}_e\bar{\mathbf{H}}_{xm^+} &= \eta_0\boldsymbol{T}_e\bar{\mathbf{H}}_{xm^-} \\ &+ \eta_0\boldsymbol{M}_x^h\boldsymbol{\sigma}_{zxh}\boldsymbol{T}_h\bar{\mathbf{E}}_{xm} - j\eta_0\boldsymbol{\sigma}_{xxe}\boldsymbol{T}_e\left(-j\bar{\mathbf{E}}_{zm}\right) \end{aligned} \tag{50}$$

By multiplying both sides of (49) by $\boldsymbol{T}_h^{-1}$, and multiplying (50) by $\boldsymbol{T}_e^{-1}$, we then have:

$$-j\eta_0\bar{\mathbf{H}}_{zm^+} = -j\eta_0\bar{\mathbf{H}}_{zm^-} - j\eta_0\boldsymbol{T}_h^{-1}\boldsymbol{\sigma}_{xxh}\boldsymbol{T}_h\bar{\mathbf{E}}_{xm} + \eta_0\boldsymbol{T}_h^{-1}\boldsymbol{M}_x^e\boldsymbol{\sigma}_{zxe}\boldsymbol{T}_e\left(-j\bar{\mathbf{E}}_{zm}\right) \quad (51)$$

$$\eta_0\bar{\mathbf{H}}_{xm^+} = \eta_0\bar{\mathbf{H}}_{xm^-} + \eta_0\boldsymbol{T}_e^{-1}\boldsymbol{M}_x^h\boldsymbol{\sigma}_{zxh}\boldsymbol{T}_h\bar{\mathbf{E}}_{xm} - j\eta_0\boldsymbol{T}_e^{-1}\boldsymbol{\sigma}_{xxe}\boldsymbol{T}_e\left(-j\bar{\mathbf{E}}_{zm}\right) \quad (52)$$

which, in matrix form, it is written as:

$$\begin{bmatrix} -j\eta_0\bar{\mathbf{H}}_{zm^+} \\ \eta_0\bar{\mathbf{H}}_{xm^+} \end{bmatrix} = \begin{bmatrix} -j\eta_0\bar{\mathbf{H}}_{zm^-} \\ \eta_0\bar{\mathbf{H}}_{xm^-} \end{bmatrix} + \begin{bmatrix} -j\eta_0\boldsymbol{T}_h^{-1}\boldsymbol{\sigma}_{xxh}\boldsymbol{T}_h & +\eta_0\boldsymbol{T}_h^{-1}\boldsymbol{M}_x^e\boldsymbol{\sigma}_{zxe}\boldsymbol{T}_e \\ \eta_0\boldsymbol{T}_e^{-1}\boldsymbol{M}_x^h\boldsymbol{\sigma}_{zxh}\boldsymbol{T}_h & -j\eta_0\boldsymbol{T}_e^{-1}\boldsymbol{\sigma}_{xxe}\boldsymbol{T}_e \end{bmatrix} \begin{bmatrix} \bar{\mathbf{E}}_{xm} \\ -j\bar{\mathbf{E}}_{zm} \end{bmatrix} \quad (53)$$

From the following definitions:

$$\bar{\mathbf{E}} = \begin{bmatrix} \bar{\mathbf{E}}_x \\ -j\bar{\mathbf{E}}_z \end{bmatrix} \bar{\mathbf{H}} = \eta_0 \begin{bmatrix} -j\bar{\mathbf{H}}_z \\ \bar{\mathbf{H}}_x \end{bmatrix} \quad (54)$$

Equation (53) can be written as:

$$\bar{\mathbf{H}}_{m^+} = \bar{\mathbf{H}}_{m^-} + \begin{bmatrix} -j\eta_0\boldsymbol{T}_h^{-1}\boldsymbol{\sigma}_{xxh}\boldsymbol{T}_h & \eta_0\boldsymbol{T}_h^{-1}\boldsymbol{M}_x^e\boldsymbol{\sigma}_{zxe}\boldsymbol{T}_e \\ \eta_0\boldsymbol{T}_e^{-1}\boldsymbol{M}_x^h\boldsymbol{\sigma}_{zxh}\boldsymbol{T}_h & -j\eta_0\boldsymbol{T}_e^{-1}\boldsymbol{\sigma}_{xxe}\boldsymbol{T}_e \end{bmatrix} \bar{\mathbf{E}}_m \quad (55)$$

$$\bar{\mathbf{H}}_{m^+} = \bar{\mathbf{H}}_{m^-} + \bar{\boldsymbol{Y}}_{gm}\bar{\mathbf{E}}_m \quad (56)$$

where

$$\bar{\boldsymbol{Y}}_{gm} = \begin{bmatrix} -j\eta_0\boldsymbol{T}_h^{-1}\boldsymbol{\sigma}_{xxh}\boldsymbol{T}_h & \eta_0\boldsymbol{T}_h^{-1}\boldsymbol{M}_x^e\boldsymbol{\sigma}_{zxe}\boldsymbol{T}_e \\ \eta_0\boldsymbol{T}_e^{-1}\boldsymbol{M}_x^h\boldsymbol{\sigma}_{zxh}\boldsymbol{T}_h & -j\eta_0\boldsymbol{T}_e^{-1}\boldsymbol{\sigma}_{xxe}\boldsymbol{T}_e \end{bmatrix} \quad (57)$$

It is assumed that by starting from the bottom of the structure and appropriate admittance transformation, $\bar{\mathbf{H}}_{m^-}$ is computed as:

$$\bar{\mathbf{H}}_{m^-} = \bar{\boldsymbol{Y}}_{tm^-}\bar{\mathbf{E}}_{m^-} = \bar{\boldsymbol{Y}}_{tm^-}\bar{\mathbf{E}}_m \quad (58)$$

By substitution of this term in (56) we have:

$$\bar{\mathbf{H}}_{m^+} = \bar{\boldsymbol{Y}}_{tm^-}\bar{\mathbf{E}}_m + \bar{\boldsymbol{Y}}_{gm}\bar{\mathbf{E}}_m = \left(\bar{\boldsymbol{Y}}_{tm^-} + \bar{\boldsymbol{Y}}_{gm}\right)\bar{\mathbf{E}}_m = \bar{\boldsymbol{Y}}_{tm^+}\bar{\mathbf{E}}_m \quad (59)$$

Hence the admittance matrix above the interface $\left(\bar{\boldsymbol{Y}}_{tm^+}\right)$ is calculated with respect to the admittance matrix below the interface $\left(\bar{\boldsymbol{Y}}_{tm^-}\right)$:

$$\bar{\boldsymbol{Y}}_{tm^+} = \bar{\boldsymbol{Y}}_{tm^-} + \bar{\boldsymbol{Y}}_{gm} \quad (60)$$

As a result, the admittance transformation at the graphene-contained interface is performed by (60). Notice that in the case that the graphene plate has not covered the entire interface, (60) can still be used for admittance transformation. To do so, the values of conductivity for the lines which are not on the graphene plate are considered zero.

C. OBTAINING THE CHARACTERISTIC EQUATION USING GRAPHENE PLATE

In the method of lines, for the analysis of the eigenmodes of a structure, the impedance and admittance are transformed from both sides of the structure. Finally, by writing the boundary conditions on a plate, the characteristic equation is obtained. The question which arises is that if this plate contains graphene, what would be the characteristic equation. As seen in Fig. 3, the graphene-contained interface has number k if counted from the bottom of the structure and has the number l if counted from the top of the structure. In other words, the fields m^- and m^+ are related to the numbers k and l, respectively. The boundary condition on the graphene-contained interface is:

$$\hat{y} \times \left(\vec{H}_l - \vec{H}_k\right) = \vec{J}_{s,m} \quad (61)$$

By expanding the fields and the current, we have:

$$\hat{y} \times \left(H_{x,l}\hat{x} + H_{z,l}\hat{z} - H_{x,k}\hat{x} - H_{z,k}\hat{z}\right) = J_{x,m}\hat{x} + J_{z,m}\hat{z} \quad (62)$$

The above equation is rewritten as:

$$\eta_0 \begin{bmatrix} -jH_{z,k} \\ H_{x,k} \end{bmatrix} - \eta_0 \begin{bmatrix} -jH_{z,l} \\ H_{x,l} \end{bmatrix} = \eta_0 \begin{bmatrix} jJ_{x,m} \\ J_{z,m} \end{bmatrix} \quad (63)$$

The position of the discretization for H_z and J_x are the same and the matrix $\boldsymbol{T}_h$ is used to transform these quantities. The same is true for the discretization of H_x and J_z. Accordingly, the matrix $\boldsymbol{T}_e$ is used to transform these quantities. If the fields are discretized, the first row of (63) is multiplied by $\boldsymbol{T}_h$, and the second row is multiplied by $\boldsymbol{T}_e$, this equation can be written in the transformed domain as:

$$\eta_0 \begin{bmatrix} -j\bar{\mathbf{H}}_{z,k} \\ \bar{\mathbf{H}}_{x,k} \end{bmatrix} - \eta_0 \begin{bmatrix} -j\bar{\mathbf{H}}_{z,l} \\ \bar{\mathbf{H}}_{x,l} \end{bmatrix} = \eta_0 \begin{bmatrix} j\bar{J}_{x,m} \\ \bar{J}_{z,m} \end{bmatrix} \quad (64)$$

From the definitions $\bar{\mathbf{H}} = \eta_0 \begin{bmatrix} -j\bar{\mathbf{H}}_z \\ \bar{\mathbf{H}}_x \end{bmatrix}$ and $\bar{J} = \eta_0 \begin{bmatrix} j\bar{J}_x \\ \bar{J}_z \end{bmatrix}$, (72) is written as follows:

$$\bar{\mathbf{H}}_k - \bar{\mathbf{H}}_l = \bar{J}_m \quad (65)$$

Starting from the bottom and top of the structure, and applying an admittance transformation to the graphene-contained interface, the fields are obtained as:

$$\bar{\mathbf{H}}_k = \bar{\boldsymbol{Y}}_{tk}\bar{\mathbf{E}}_m, \bar{\mathbf{H}}_l = -\bar{\boldsymbol{Y}}_{tl}\bar{\mathbf{E}}_m \quad (66)$$

By substitution of these expressions into (65) we have:

$$\left(\bar{\boldsymbol{Y}}_{tk} + \bar{\boldsymbol{Y}}_{tl}\right)\bar{\mathbf{E}}_m = \bar{J}_m \quad (67)$$

$$\left(\bar{\boldsymbol{Y}}_{tk} + \bar{\boldsymbol{Y}}_{tl}\right)^{-1}\bar{J}_m = \bar{\mathbf{E}}_m \quad (68)$$

Since admittance transformation is done at the transformed domain, (67) and (68) are also obtained in the transformed domain. To apply appropriate boundary conditions and obtain the characteristic equation, these equations should be written

in the space domain, thus (68) in the space domain is written as:

$$\begin{bmatrix} \boldsymbol{T}_h & \mathbf{0} \\ \mathbf{0} & \boldsymbol{T}_e \end{bmatrix} \begin{bmatrix} \bar{Z}_{11} & \bar{Z}_{12} \\ \bar{Z}_{21} & \bar{Z}_{22} \end{bmatrix} \begin{bmatrix} \boldsymbol{T}_h^t & \mathbf{0} \\ \mathbf{0} & \boldsymbol{T}_e^t \end{bmatrix} \times \begin{bmatrix} j\eta_0 \mathbf{J}_{x,m} \\ \eta_0 \mathbf{J}_{z,m} \end{bmatrix} = \begin{bmatrix} \mathbf{E}_{x,m} \\ -j\mathbf{E}_{z,m} \end{bmatrix} \tag{69}$$

$$\begin{bmatrix} \mathbf{Z}_{11} & \mathbf{Z}_{12} \\ \mathbf{Z}_{21} & \mathbf{Z}_{22} \end{bmatrix} \begin{bmatrix} j\eta_0 \mathbf{J}_{x,m} \\ \eta_0 \mathbf{J}_{z,m} \end{bmatrix} = \begin{bmatrix} \mathbf{E}_{x,m} \\ -j\mathbf{E}_{z,m} \end{bmatrix} \tag{70}$$

The current and electric field vectors at the plane m in the microstrip line shown in Fig. 4, are as follows:

$$\mathbf{J}_m = \eta_0 \begin{bmatrix} \mathbf{0_{x,ls}} \\ j\mathbf{J}_{x,g} \\ \mathbf{0_{x,rs}} \\ \mathbf{0_{z,ls}} \\ \mathbf{J}_{z,g} \\ \mathbf{0_{z,rs}} \end{bmatrix} \mathbf{E}_m = \begin{bmatrix} \mathbf{E}_{x,ls} \\ \mathbf{E}_{x,g} \\ \mathbf{E}_{x,rs} \\ -j\mathbf{E}_{z,ls} \\ -j\mathbf{E}_{z,g} \\ -j\mathbf{E}_{z,rs} \end{bmatrix} \tag{71}$$

The g index in the above quantities indicates the lines on the graphene plate, the index ls indicates the lines located in the slot region at the left side of the graphene plate, and rs indicates the lines located in the slot region at the right side of the graphene plate. Regarding the zero components of the current vector, columns of $\mathbf{Z}$ in (70) which are multiplied by these components can be omitted and the matrix can be reduced to:

$$\begin{bmatrix} \mathbf{Z}_{11}^{r,ls} & \mathbf{Z}_{12}^{r,ls} \\ \mathbf{Z}_{11}^{r,g} & \mathbf{Z}_{12}^{r,g} \\ \mathbf{Z}_{11}^{r,rs} & \mathbf{Z}_{12}^{r,rs} \\ \mathbf{Z}_{21}^{r,ls} & \mathbf{Z}_{22}^{r,ls} \\ \mathbf{Z}_{21}^{r,g} & \mathbf{Z}_{22}^{r,g} \\ \mathbf{Z}_{21}^{r,rs} & \mathbf{Z}_{22}^{r,rs} \end{bmatrix} \begin{bmatrix} j\eta_0 \mathbf{J}_{x,g} \\ \eta_0 \mathbf{J}_{z,g} \end{bmatrix} = \begin{bmatrix} \mathbf{E}_{x,ls} \\ \mathbf{E}_{x,g} \\ \mathbf{E}_{x,rs} \\ -j\mathbf{E}_{z,ls} \\ -j\mathbf{E}_{z,g} \\ -j\mathbf{E}_{z,rs} \end{bmatrix} \tag{72}$$

After reducing $\mathbf{Z}$ matrix, the vector on the right hand side of (72) contains the field components either in the slot regions or on the graphene plate. Hence the submatrices can be divided into left slot (ls), right slot (rs), and graphene plate (g) groups. Therefore, (72) can be decomposed into three equations, as follows:

$$\begin{bmatrix} \mathbf{Z}_{11}^{r,ls} & \mathbf{Z}_{12}^{r,ls} \\ \mathbf{Z}_{21}^{r,ls} & \mathbf{Z}_{22}^{r,ls} \end{bmatrix} \begin{bmatrix} j\eta_0 \mathbf{J}_{x,g} \\ \eta_0 \mathbf{J}_{z,g} \end{bmatrix} = \begin{bmatrix} \mathbf{E}_{x,ls} \\ -j\mathbf{E}_{z,ls} \end{bmatrix} \tag{73}$$

$$\begin{bmatrix} \mathbf{Z}_{11}^{r,g} & \mathbf{Z}_{12}^{r,g} \\ \mathbf{Z}_{21}^{r,g} & \mathbf{Z}_{22}^{r,g} \end{bmatrix} \begin{bmatrix} j\eta_0 \mathbf{J}_{x,g} \\ \eta_0 \mathbf{J}_{z,g} \end{bmatrix} = \begin{bmatrix} \mathbf{E}_{x,g} \\ -j\mathbf{E}_{z,g} \end{bmatrix} \tag{74}$$

$$\begin{bmatrix} \mathbf{Z}_{11}^{r,rs} & \mathbf{Z}_{12}^{r,rs} \\ \mathbf{Z}_{21}^{r,rs} & \mathbf{Z}_{22}^{r,rs} \end{bmatrix} \begin{bmatrix} j\eta_0 \mathbf{J}_{x,g} \\ \eta_0 \mathbf{J}_{z,g} \end{bmatrix} = \begin{bmatrix} \mathbf{E}_{x,rs} \\ -j\mathbf{E}_{z,rs} \end{bmatrix} \tag{75}$$

The current on the graphene plate is calculated as:

$$\begin{bmatrix} \mathrm{J}_x \\ \mathrm{J}_z \end{bmatrix} = \begin{bmatrix} \sigma_{xx} E_x + \sigma_{zx} E_z \\ -\sigma_{zx} E_x + \sigma_{xx} E_z \end{bmatrix} = \begin{bmatrix} \sigma_{xx} & \sigma_{zx} \\ -\sigma_{zx} & \sigma_{xx} \end{bmatrix} \begin{bmatrix} E_x \\ E_z \end{bmatrix} = \overline{\overline{\sigma}}. \begin{bmatrix} E_x \\ E_z \end{bmatrix} \tag{76}$$

The current vector in the discretized form is as follows:

$$\begin{bmatrix} j\eta_0 \mathbf{J}_{x,g} \\ \eta_0 \mathbf{J}_{z,g} \end{bmatrix} = \begin{bmatrix} j\eta_0 \boldsymbol{\sigma}_{xx,h}^{g} & -\eta_0 \left(\boldsymbol{M}_x^e \boldsymbol{\sigma}_{zx,e}\right)^g \\ -\eta_0 \left(\boldsymbol{M}_x^h \boldsymbol{\sigma}_{zx,h}\right)^g & j\eta_0 \boldsymbol{\sigma}_{xx,e}^{g} \end{bmatrix} \begin{bmatrix} \mathbf{E}_{x,g} \\ -j\mathbf{E}_{z,g} \end{bmatrix} \tag{77}$$

It should be noted that the positions of the field components are different from each other, for instance, in (77) the E_x components are discretized at different positions than those of E_z components, and hence these components cannot be added or subtracted from each other directly. To overcome this problem, the interpolation matrices have been utilized in (77) to obtain the values of the terms $\boldsymbol{\sigma}_{zxh}\mathbf{E}_{x,g}$ and $\boldsymbol{\sigma}_{zxe}\left(-j\mathbf{E}_{z,g}\right)$ at the correct position.

By substituting (77) into (74), we have:

$$\begin{bmatrix} \mathbf{Z}_{11}^{r,g} & \mathbf{Z}_{12}^{r,g} \\ \mathbf{Z}_{21}^{r,g} & \mathbf{Z}_{22}^{r,g} \end{bmatrix} \begin{bmatrix} j\eta_0 \boldsymbol{\sigma}_{xxh}^{g} & -\eta_0 \left(\boldsymbol{M}_x^e \boldsymbol{\sigma}_{zxe}\right)^g \\ -\eta_0 \left(\boldsymbol{M}_x^h \boldsymbol{\sigma}_{zxh}\right)^g & j\eta_0 \boldsymbol{\sigma}_{xxe}^{g} \end{bmatrix} \begin{bmatrix} \mathbf{E}_{x,g} \\ -j\mathbf{E}_{z,g} \end{bmatrix} = \begin{bmatrix} \mathbf{E}_{x,g} \\ -j\mathbf{E}_{z,g} \end{bmatrix} \tag{78}$$

In the above equation the superscript g denotes that all the quantities are on the discretization lines on the graphene plate. Equation (78) is rewritten in the following homogeneous form:

$$\left(\begin{bmatrix} \mathbf{Z}_{11}^{r,g} & \mathbf{Z}_{12}^{r,g} \\ \mathbf{Z}_{21}^{r,g} & \mathbf{Z}_{22}^{r,g} \end{bmatrix} \begin{bmatrix} j\eta_0 \boldsymbol{\sigma}_{xxh}^{g} & -\eta_0 \left(\boldsymbol{M}_x^e \boldsymbol{\sigma}_{zxe}\right)^g \\ -\eta_0 \left(\boldsymbol{M}_x^h \boldsymbol{\sigma}_{zxh}\right)^g & j\eta_0 \boldsymbol{\sigma}_{xxe}^{g} \end{bmatrix} - \begin{bmatrix} \mathbf{I}_{x,g} & \mathbf{0} \\ \mathbf{0} & \mathbf{I}_{z,g} \end{bmatrix} \right) \begin{bmatrix} \mathbf{E}_{x,g} \\ -j\mathbf{E}_{z,g} \end{bmatrix} = \mathbf{0} \tag{79}$$

$\mathbf{I}_{x,g}$ and $\mathbf{I}_{z,g}$ are unity matrices with their dimensions being equal to the number of dashed and solid lines positioned on the graphene plate, respectively. In order for (79) to have a non-zero solution, the determinant of the coefficients matrix must be zero, hence the characteristic equation is obtained as:

$$\det\left(\begin{bmatrix} \mathbf{Z}_{11}^{r,g} & \mathbf{Z}_{12}^{r,g} \\ \mathbf{Z}_{21}^{r,g} & \mathbf{Z}_{22}^{r,g} \end{bmatrix} \begin{bmatrix} j\eta_0 \boldsymbol{\sigma}_{xxh}^{g} & -\eta_0 \boldsymbol{M}_x^{eg} \boldsymbol{\sigma}_{xxh}^{g} \\ -\eta_0 \boldsymbol{M}_x^{hg} \boldsymbol{\sigma}_{zxh}^{g} & j\eta_0 \boldsymbol{\sigma}_{xxe}^{g} \end{bmatrix} - \begin{bmatrix} \mathbf{I}_{x,g} & \mathbf{0} \\ \mathbf{0} & \mathbf{I}_{z,g} \end{bmatrix} \right) = 0 \tag{80}$$

For the microstrip line, ε_{re} is obtained from the above equation.

An alternative way to get the characteristic equation is using (67). In this way, we do not need to inverse the matrix $\left(\bar{\boldsymbol{Y}}_{tk} + \bar{\boldsymbol{Y}}_{tl}\right)$. Equation (67) is written as:

$$\left(\bar{\boldsymbol{Y}}_{tk} + \bar{\boldsymbol{Y}}_{tl}\right) \bar{\mathbf{E}}_m = \bar{J}_m \tag{81}$$

$$\begin{bmatrix} \boldsymbol{T}_h & \mathbf{0} \\ \mathbf{0} & \boldsymbol{T}_e \end{bmatrix} \begin{bmatrix} \bar{\boldsymbol{Y}}_{11} & \bar{\boldsymbol{Y}}_{12} \\ \bar{\boldsymbol{Y}}_{21} & \bar{\boldsymbol{Y}}_{22} \end{bmatrix} \begin{bmatrix} \boldsymbol{T}_h^t & \mathbf{0} \\ \mathbf{0} & \boldsymbol{T}_e^t \end{bmatrix} \times \begin{bmatrix} \mathbf{E}_{x,m} \\ -j\mathbf{E}_{z,m} \end{bmatrix} = \begin{bmatrix} j\eta_0 \mathbf{J}_{x,m} \\ \eta_0 \mathbf{J}_{z,m} \end{bmatrix} \tag{82}$$

$$\begin{bmatrix} \mathbf{Y}_{11} & \mathbf{Y}_{12} \\ \mathbf{Y}_{21} & \mathbf{Y}_{22} \end{bmatrix} \begin{bmatrix} \mathbf{E}_{x,m} \\ -j\mathbf{E}_{z,m} \end{bmatrix} = \begin{bmatrix} j\eta_0 \mathbf{J}_{x,m} \\ \eta_0 \mathbf{J}_{z,m} \end{bmatrix} \tag{83}$$

Using (71), (83) is written as the following:

$$\begin{bmatrix} \mathbf{y}_{11} & \mathbf{y}_{12} & \mathbf{y}_{13} & \mathbf{y}_{14} & \mathbf{y}_{15} & \mathbf{y}_{16} \\ \mathbf{y}_{21} & \mathbf{y}_{22} & \mathbf{y}_{23} & \mathbf{y}_{24} & \mathbf{y}_{25} & \mathbf{y}_{26} \\ \mathbf{y}_{31} & \mathbf{y}_{32} & \mathbf{y}_{33} & \mathbf{y}_{34} & \mathbf{y}_{35} & \mathbf{y}_{36} \\ \mathbf{y}_{41} & \mathbf{y}_{42} & \mathbf{y}_{43} & \mathbf{y}_{44} & \mathbf{y}_{45} & \mathbf{y}_{46} \\ \mathbf{y}_{51} & \mathbf{y}_{52} & \mathbf{y}_{53} & \mathbf{y}_{54} & \mathbf{y}_{55} & \mathbf{y}_{56} \\ \mathbf{y}_{61} & \mathbf{y}_{62} & \mathbf{y}_{63} & \mathbf{y}_{64} & \mathbf{y}_{65} & \mathbf{y}_{66} \end{bmatrix} \begin{bmatrix} \mathbf{E}_{x,ls} \\ \mathbf{E}_{x,g} \\ \mathbf{E}_{x,rs} \\ -j\mathbf{E}_{z,ls} \\ -j\mathbf{E}_{z,g} \\ -j\mathbf{E}_{z,rs} \end{bmatrix} = \eta_0 \begin{bmatrix} \mathbf{0_{x,ls}} \\ j\mathbf{J}_{x,g} \\ \mathbf{0_{x,rs}} \\ \mathbf{0_{z,ls}} \\ \mathbf{J}_{z,g} \\ \mathbf{0_{z,rs}} \end{bmatrix} \tag{84}$$

This equation can be decomposed into three equations:

$$\begin{bmatrix} \mathbf{y}_{11} & \mathbf{y}_{12} & \mathbf{y}_{13} & \mathbf{y}_{14} & \mathbf{y}_{15} & \mathbf{y}_{16} \\ \mathbf{y}_{41} & \mathbf{y}_{42} & \mathbf{y}_{43} & \mathbf{y}_{44} & \mathbf{y}_{45} & \mathbf{y}_{46} \end{bmatrix} \begin{bmatrix} \mathbf{E}_{x,ls} \\ \mathbf{E}_{x,g} \\ \mathbf{E}_{x,rs} \\ -j\mathbf{E}_{z,ls} \\ -j\mathbf{E}_{z,g} \\ -j\mathbf{E}_{z,rs} \end{bmatrix} = \begin{bmatrix} \mathbf{0_{x,ls}} \\ \mathbf{0_{z,ls}} \end{bmatrix} \tag{85}$$

$$\begin{bmatrix} \mathbf{y}_{21} & \mathbf{y}_{22} & \mathbf{y}_{23} & \mathbf{y}_{24} & \mathbf{y}_{25} & \mathbf{y}_{26} \\ \mathbf{y}_{51} & \mathbf{y}_{52} & \mathbf{y}_{53} & \mathbf{y}_{44} & \mathbf{y}_{55} & \mathbf{y}_{56} \end{bmatrix} \begin{bmatrix} \mathbf{E}_{x,ls} \\ \mathbf{E}_{x,g} \\ \mathbf{E}_{x,rs} \\ -j\mathbf{E}_{z,ls} \\ -j\mathbf{E}_{z,g} \\ -j\mathbf{E}_{z,rs} \end{bmatrix} = \eta_0 \begin{bmatrix} j\mathbf{J}_{x,g} \\ \mathbf{J}_{z,g} \end{bmatrix} \tag{86}$$

$$\begin{bmatrix} \mathbf{y}_{31} & \mathbf{y}_{32} & \mathbf{y}_{33} & \mathbf{y}_{34} & \mathbf{y}_{35} & \mathbf{y}_{36} \\ \mathbf{y}_{61} & \mathbf{y}_{62} & \mathbf{y}_{63} & \mathbf{y}_{64} & \mathbf{y}_{65} & \mathbf{y}_{66} \end{bmatrix} \begin{bmatrix} \mathbf{E}_{x,ls} \\ \mathbf{E}_{x,g} \\ \mathbf{E}_{x,rs} \\ -j\mathbf{E}_{z,ls} \\ -j\mathbf{E}_{z,g} \\ -j\mathbf{E}_{z,rs} \end{bmatrix} = \begin{bmatrix} \mathbf{0_{x,rs}} \\ \mathbf{0_{z,rs}} \end{bmatrix} \tag{87}$$

These equations can be written in the following form in which the current vectors on the graphene plate are written in terms of the electric field.

$$\begin{aligned} &\begin{bmatrix} \mathbf{y}_{11} & \mathbf{y}_{14} \\ \mathbf{y}_{41} & \mathbf{y}_{44} \end{bmatrix} \begin{bmatrix} \mathbf{E}_{x,ls} \\ -j\mathbf{E}_{z,ls} \end{bmatrix} + \begin{bmatrix} \mathbf{y}_{12} & \mathbf{y}_{15} \\ \mathbf{y}_{42} & \mathbf{y}_{45} \end{bmatrix} \begin{bmatrix} \mathbf{E}_{x,g} \\ -j\mathbf{E}_{z,g} \end{bmatrix} \\ &+ \begin{bmatrix} \mathbf{y}_{13} & \mathbf{y}_{16} \\ \mathbf{y}_{43} & \mathbf{y}_{46} \end{bmatrix} \begin{bmatrix} \mathbf{E}_{x,rs} \\ -j\mathbf{E}_{z,rs} \end{bmatrix} = \begin{bmatrix} \mathbf{0_{x,ls}} \\ \mathbf{0_{z,ls}} \end{bmatrix} \\ &\begin{bmatrix} \mathbf{y}_{21} & \mathbf{y}_{24} \\ \mathbf{y}_{51} & \mathbf{y}_{54} \end{bmatrix} \begin{bmatrix} \mathbf{E}_{x,ls} \\ -j\mathbf{E}_{z,ls} \end{bmatrix} + \begin{bmatrix} \mathbf{y}_{22} & \mathbf{y}_{25} \\ \mathbf{y}_{52} & \mathbf{y}_{55} \end{bmatrix} \begin{bmatrix} \mathbf{E}_{x,g} \\ -j\mathbf{E}_{z,g} \end{bmatrix} \\ &+ \begin{bmatrix} \mathbf{y}_{23} & \mathbf{y}_{26} \\ \mathbf{y}_{53} & \mathbf{y}_{56} \end{bmatrix} \begin{bmatrix} \mathbf{E}_{x,rs} \\ -j\mathbf{E}_{z,rs} \end{bmatrix} \end{aligned} \tag{88}$$

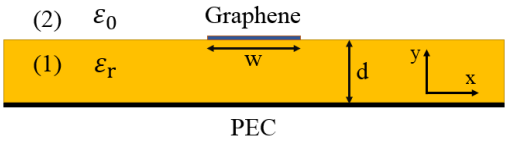

FIGURE 5. Microstrip transmission line with the graphene sheet used as the strip.

$$= \begin{bmatrix} j\eta_0\boldsymbol{\sigma}^g_{xx,h} & -\eta_0\left(\boldsymbol{M}^e_x\boldsymbol{\sigma}_{zx,e}\right)^g \\ -\eta_0\left(\boldsymbol{M}^h_x\boldsymbol{\sigma}_{zx,h}\right)^g & j\eta_0\boldsymbol{\sigma}^g_{xx,e} \end{bmatrix} \begin{bmatrix} \mathbf{E}_{x,g} \\ -j\mathbf{E}_{z,g} \end{bmatrix} \tag{89}$$

$$\begin{bmatrix} \mathbf{y}_{31} & \mathbf{y}_{34} \\ \mathbf{y}_{61} & \mathbf{y}_{64} \end{bmatrix} \begin{bmatrix} \mathbf{E}_{x,ls} \\ -j\mathbf{E}_{z,ls} \end{bmatrix} + \begin{bmatrix} \mathbf{y}_{32} & \mathbf{y}_{35} \\ \mathbf{y}_{62} & \mathbf{y}_{65} \end{bmatrix} \begin{bmatrix} \mathbf{E}_{x,g} \\ -j\mathbf{E}_{z,g} \end{bmatrix} + \begin{bmatrix} \mathbf{y}_{33} & \mathbf{y}_{36} \\ \mathbf{y}_{63} & \mathbf{y}_{66} \end{bmatrix} \begin{bmatrix} \mathbf{E}_{x,rs} \\ -j\mathbf{E}_{z,rs} \end{bmatrix} = \begin{bmatrix} \mathbf{0_{x,rs}} \\ \mathbf{0_{z,rs}} \end{bmatrix} \tag{90}$$

These equations are rewritten in a summary form as:

$$\mathbf{A}\left[\mathbf{E}_{ls}\right] + \mathbf{B}\left[\mathbf{E}_g\right] + \mathbf{C}\left[\mathbf{E}_{rs}\right] = \left[\mathbf{0_{ls}}\right] \tag{91}$$

$$\boldsymbol{D}\left[\mathbf{E}_{ls}\right] + \mathbf{E}\left[\mathbf{E}_g\right] + \boldsymbol{F}\left[\mathbf{E}_{rs}\right] = \boldsymbol{\sigma}\left[\mathbf{E}_g\right] \tag{92}$$

$$\mathbf{G}\left[\mathbf{E}_{ls}\right] + \mathbf{H}\left[\mathbf{E}_g\right] + \boldsymbol{I}\left[\mathbf{E}_{rs}\right] = \left[\mathbf{0_{rs}}\right] \tag{93}$$

The vectors $[\mathbf{E}_{ls}]$ and $[\mathbf{E}_{rs}]$ are obtained from (91) and (93) as the following:

$$\begin{aligned} \left[\mathbf{E}_{rs}\right] &= \left[-\mathbf{G}\mathbf{A}^{-1}\mathbf{C} + \mathbf{I}\right]^{-1}\left[\mathbf{G}\mathbf{A}^{-1}\mathbf{B} - \mathbf{H}\right]\left[\mathbf{E}_g\right] \\ &= \boldsymbol{M}_1\left[\mathbf{E}_g\right] \end{aligned} \tag{94}$$

$$\begin{aligned} \left[\mathbf{E}_{ls}\right] = &\left[-\mathbf{A}^{-1}\mathbf{B} + \mathbf{A}^{-1}\mathbf{C}\left[-\mathbf{G}\mathbf{A}^{-1}\mathbf{C} + \mathbf{I}\right]^{-1}\right. \\ &\left.\times\left[-\mathbf{G}\mathbf{A}^{-1}\mathbf{B} + \mathbf{H}\right]\right]\left[\mathbf{E}_g\right] = \boldsymbol{M}_2\left[\mathbf{E}_g\right] \end{aligned} \tag{95}$$

By substituting (94) and (95) into (92) we have:

$$\left[\boldsymbol{D}\boldsymbol{M}_1 + \mathbf{E} + \boldsymbol{F}\boldsymbol{M}_2\right]\left[\mathbf{E}_g\right] = \boldsymbol{\sigma}\left[\mathbf{E}_g\right] \tag{96}$$

Therefore, the characteristic equation takes the form:

$$det\left[\boldsymbol{D}\boldsymbol{M}_1 + \mathbf{E} + \boldsymbol{F}\boldsymbol{M}_2 - \boldsymbol{\sigma}\right] = 0 \tag{97}$$

The solutions of the characteristic equations (80) and (97) are the same. The propagation constant is as the following:

$$k_z = \sqrt{\varepsilon}_{eff} = k_{zr} - jk_{zi} \tag{98}$$

D. SPECTRAL DOMAIN METHOD FOR THE ANALYSIS OF GRAPHENE-BASED MICROSTRIP LINE

Spectral Domain Method is one of the best methods for the analysis of planar transmission lines. It uses Fourier transformation of the fields to solve the integral equations. Generalized formulations of this method for the analysis of planar microstrip transmission lines are presented in [23]. Following the aforesaid formulations, we briefly describe the way to analyze a microstrip transmission line structure with a graphene slab (Fig. 5).

The fields are calculated as the superposition of the Fourier form of TE-to-y and TM-to-y expressions derived from the Fourier transformed scalar potentials $\tilde{\psi}^e$and $\tilde{\psi}^h$[23]. Solving the Fourier-transformed Helmholtz equation for both

scalar potentials considering the boundary conditions of the problem, the following solutions can be assumed for the regions 1 and 2 specified in Fig. 5:

Region 1 (considering zero tangential fields at $y = 0$):

$$\tilde{\psi}^e = B^e \cosh(\gamma_1 y) \tag{99}$$

$$\tilde{\psi}^h = B^h \sinh(\gamma_1 y) \tag{100}$$

Region 2 (considering zero fields at infinity):

$$\tilde{\psi}^e = A^e e^{-\gamma_2 y} \tag{101}$$

$$\tilde{\psi}^h = A^h e^{-\gamma_2 y} \tag{102}$$

where $A^e, A^h, B^e, B^h$are unknown coefficients and $\gamma_i = \sqrt{\alpha^2 + \beta^2 - k_i^2}$ is the propagation constant in y direction. Substitution of the assumed solutions into the TE-to-y and TM-to-y Fourier form expressions, yields the generalized form of the fields in the two regions including the unknown coefficients [24, eqs. (18)–(28)]. It is well known that the space domain boundary conditions at the graphene-contained interfaces include the continuity of the tangential components of electric field, and the jumping of the tangential components of magnetic field by the corresponding unknown graphene current density component. Using the space domain boundary conditions at y = d, the unknown coefficients are determined, and the following relations are obtained:

$$\begin{bmatrix} \tilde{E}_{z1} \\ \tilde{E}_{x1} \end{bmatrix} = \begin{bmatrix} Z_{zz} & Z_{zx} \\ Z_{xz} & Z_{xx} \end{bmatrix} \begin{bmatrix} \tilde{J}_z \\ \tilde{J}_x \end{bmatrix} \tag{103}$$

in which

$$Z_{xx} = \frac{1}{\alpha^2 + \beta^2} \left(-\alpha^2 Z^e - \beta^2 Z^h \right) \tag{104}$$

$$Z_{zz} = \frac{1}{\alpha^2 + \beta^2} \left(-\beta^2 Z^e - \alpha^2 Z^h \right) \tag{105}$$

$$Z_{xz} = Z_{xz} = \frac{\alpha\beta}{\alpha^2 + \beta^2} \left(-Z^e + Z^h \right) \tag{106}$$

where

$$Z^e = \frac{\gamma_1 \gamma_2}{\gamma_2 \hat{y}_1 \coth(d\gamma_1) + \gamma_1 \hat{y}_2} \tag{107}$$

$$Z^h = \frac{\hat{z}_1 \hat{z}_2}{\gamma_1 \hat{z}_2 \coth(d\gamma_1) + \gamma_2 \hat{z}_1} \tag{108}$$

which contains four unknowns. Assume that the spectral domain currents $\tilde{J}_x$ and $\tilde{J}_z$ are sums of N and M knows basis functions $\tilde{J}_{xm}$ and $\tilde{J}_{zm}$, respectively, with c_m and d_m being the unknown coefficients. Then, an equation based on a momentum matrix is formed [24]:

$$\begin{bmatrix} K_{km}^{(1,1)} & K_{km}^{(1,2)} \\ K_{lm}^{(2,1)} & K_{lm}^{(2,2)} \end{bmatrix} \begin{bmatrix} c_m \\ d_m \end{bmatrix} = \begin{bmatrix} e_m \\ f_m \end{bmatrix} \tag{109}$$

in which c_m, d_m, e_m and f_m are the unknowns to be determined.

As the graphene surface has a tensor conductivity, the relation between the current distributions and the tangential electric fields is:

$$\begin{bmatrix} E_z \\ E_x \end{bmatrix} = \begin{bmatrix} \frac{\sigma_{xx}}{\sigma} & -\frac{\sigma_{zx}}{\sigma} \\ \frac{\sigma_{zx}}{\sigma} & \frac{\sigma_{xx}}{\sigma} \end{bmatrix} \begin{bmatrix} J_z \\ J_x \end{bmatrix} \tag{110}$$

where

$$\sigma = \sigma_{xx}^2 + \sigma_{zx}^2 \tag{111}$$

Substitution of this relation into the equations which include e_m and f_m, results in a relation which expresses e_m and f_m in terms of $c_m$and d_m [24]:

$$\begin{bmatrix} e_m \\ f_m \end{bmatrix} = \begin{bmatrix} P_{km}^{(1,1)} & P_{km}^{(1,2)} \\ P_{lm}^{(2,1)} & P_{lm}^{(2,2)} \end{bmatrix} \begin{bmatrix} c_m \\ d_m \end{bmatrix} \tag{112}$$

As a result, the matrix equation (109) can be written as:

$$\begin{bmatrix} K_{km}^{(1,1)} - P_{km}^{(1,1)} & K_{km}^{(1,2)} - P_{km}^{(1,2)} \\ K_{lm}^{(2,1)} - P_{lm}^{(2,1)} & K_{lm}^{(2,2)} - P_{lm}^{(2,2)} \end{bmatrix} \begin{bmatrix} c_m \\ d_m \end{bmatrix} = \begin{bmatrix} 0 \\ 0 \end{bmatrix} \tag{113}$$

where c_m and d_m are the unknowns, and the propagation constant is obtained by equating the determinant of the matrix in (113) to zero. Generally, any kind of basis function can be utilized, however, in normal propagation modes symmetric basis functions could result in more accurate results [24]. On the other hand, in plasmonic propagation modes, symmetric functions cannot model the problem accurately. Hence the basis functions are chosen as a combination of sine and cosine functions.

III. SOFTWARE SIMULATION

In the previous sections, the analysis of graphene multilayered structures using the method of lines was explained, and also the analysis of graphene microstrip lines by the spectral domain method was presented. In order to verify the results obtained from these methods, the two aforesaid structures are simulated using COMSOL software. This software solves the electromagnetic waves using the finite element method and computes the electric field using Maxwell equations. The magnetic field and other quantities related to the structure are calculated from the electric field. The simulation of the three structures, i.e., graphene microstrip line, graphene stripline, and parallel-plate waveguide, is done using the COMSOL software. The analysis mode of COMSOL software is used to obtain the propagation constant of the structure. To analyze 2D structures, it is sufficient to analyze the cross section of these structures which is a plate. Figs. (6), (7) and (8) illustrate the graphene microstrip line, graphene stripline, and graphene parallel-plate waveguide in COMSOL software, respectively.

For further clarity, the zoomed state of the COMSOL is not shown. At the boundaries adjacent to the free space, PML plates are placed around the structure with an appropriate distance which is not shown in the figures. To model the graphene plate, it is considered as a material with a very low

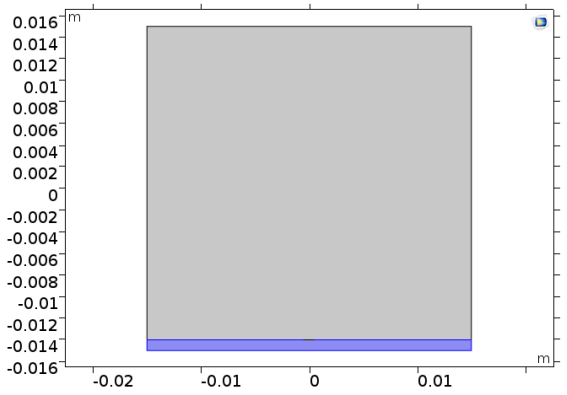

FIGURE 6. Graphene microstrip line structure in COMSOL environment (the values are in meters and the bottom rectangle is dielectric).

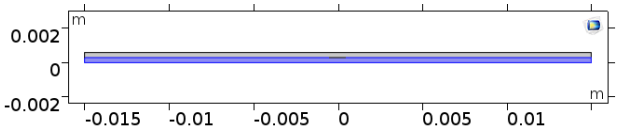

FIGURE 7. Graphene stripline structure in COMSOL environment.

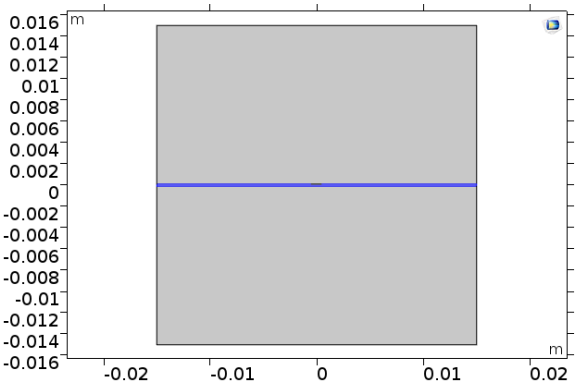

FIGURE 8. Graphene parallel-plate waveguide structure in COMSOL environment.

thickness of $t = 1\mu m$ with anisotropic permittivity as the following [24]:

$$\bar{\bar{\varepsilon}} = 1 + \bar{\bar{\sigma}}/j\omega t\varepsilon_0 \tag{114}$$

where

$$\bar{\bar{\sigma}} = \begin{bmatrix} \sigma_{zz} & 0 & -\sigma_{zz} \\ 0 & 0 & 0 \\ \sigma_{zx} & 0 & \sigma_{zz} \end{bmatrix} \tag{115}$$

in which t is the thickness of the graphene plate. Substitution of (115) in (114) gives the permittivity matrix as:

$$\bar{\bar{\varepsilon}} = \begin{bmatrix} \varepsilon_{zz} & 0 & -\varepsilon_{zz} \\ 0 & 1 & 0 \\ \varepsilon_{zx} & 0 & \varepsilon_{zz} \end{bmatrix} \tag{116}$$

where

$$\bar{\bar{\varepsilon}} = 1 + \bar{\bar{\sigma}}/j\omega t\varepsilon_0 \tag{117}$$

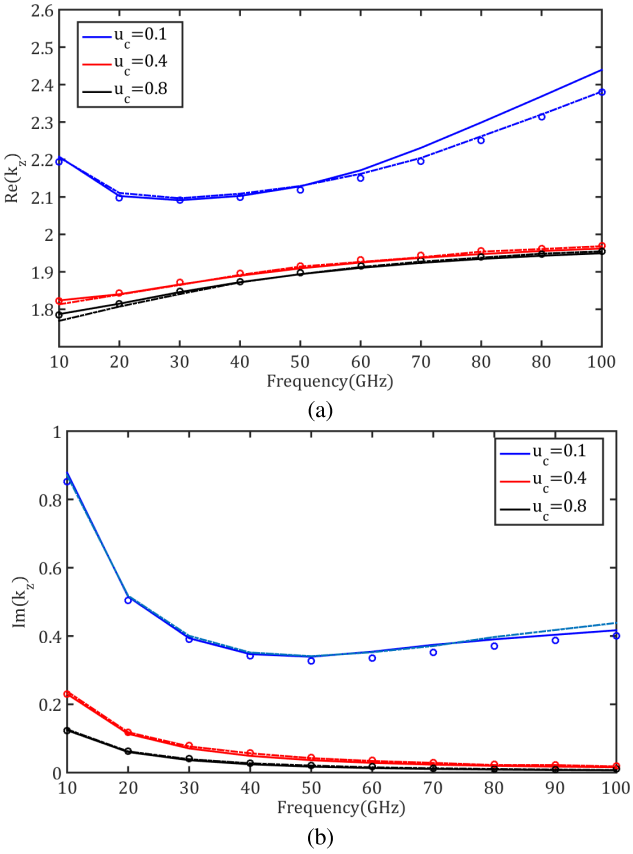

FIGURE 9. The normalized propagation constant of the microstrip line plotted for three chemical potentials and magnetic bias $B_0 = 0.1\ T$: a) real part, b) imaginary part, Solid line: SDM method, Dashed line: MOL method, Circles: COMSOL Simulation.

IV. RESULTS

As examples of multilayered structures, three structures of graphene-based microstrip line, graphene-based stripline, and graphene-based parallel-plate waveguide are analyzed using the proposed method in this paper (i.e. extended method of lines). Also, the microstrip line is analyzed using the spectral domain method. All these structures are also simulated using the COMSOL software. In this section, the results of different methods are discussed and the COMSOL software simulations are presented.

A. MICROSTRIP LINE

As the first example of graphene-contained multilayered structures, the results from the analysis of the microstrip line using the extended method of lines is presented. The structure of the graphene microstrip line is illustrated in Fig. 5. The width of the graphene strip is $w = 1mm$ and the substrate thickness is $d = 1mm$. The permittivity of the substrate and the magnetic bias of graphene are considered as $\varepsilon_r = 4$ and $B_0 = 0.1T$, respectively. The propagation constant of the microstrip line with the above-mentioned characteristics is computed using MOL and SDM methods, and is compared with COMSOL simulations. Fig. 9 plots the real and imaginary parts of the propagation constant with respect

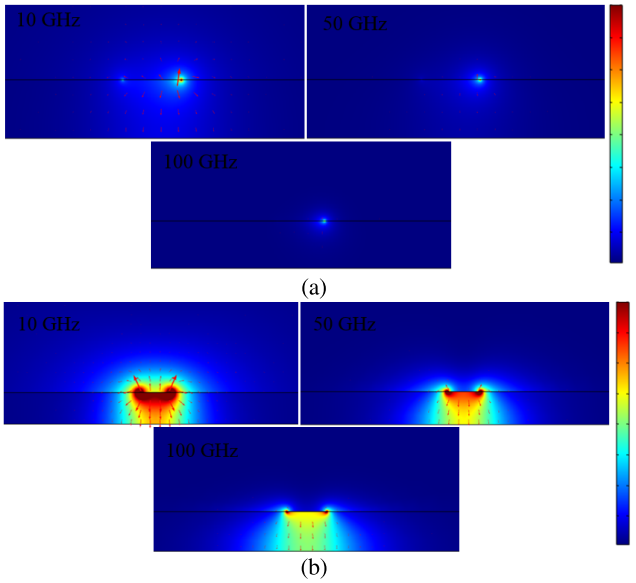

FIGURE 10. Electric field distribution for different frequencies: a) $\mu_c = 0.1$, b) $\mu_c = 0.8$.

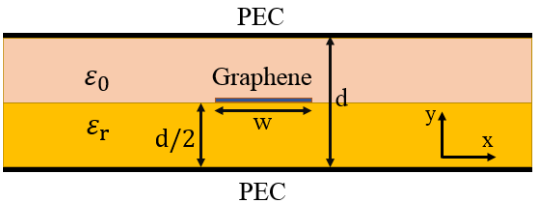

FIGURE 11. Analyzed graphene-based stripline.

to the frequency for the chemical potentials $\mu_c = 0.1ev$, $0.4ev$, $0.8ev$.

Electric field distribution of graphene microstrip line at different frequencies for different chemical potentials is shown in Fig. 10.

B. STRIPLINE

As the second example of graphene-contained multilayered structures, the analysis of the graphene stripline using the extended method of lines is presented. The structure of the graphene stripline is illustrated in Fig. 11.

The width of the graphene strip is w = 1mm and the distance between the two PEC plates is d = 0.6mm. Dielectric permittivity under the graphene plate is $\varepsilon_r = 4$ and the magnetic bias of graphene is $B_0 = 0.1T$. The propagation constant of the graphene stripline with the above-mentioned characteristics is computed using the extended method of lines, and is compared with the results of COMSOL software. Fig. 12 plots the real and imaginary parts of the propagation constant with respect to the frequency for three chemical potentials $\mu_c = 0.1ev, 0.4ev, 0.8ev$.

Electric field distribution of graphene stripline structure at different frequencies for different chemical potentials is shown in Fig. 13.

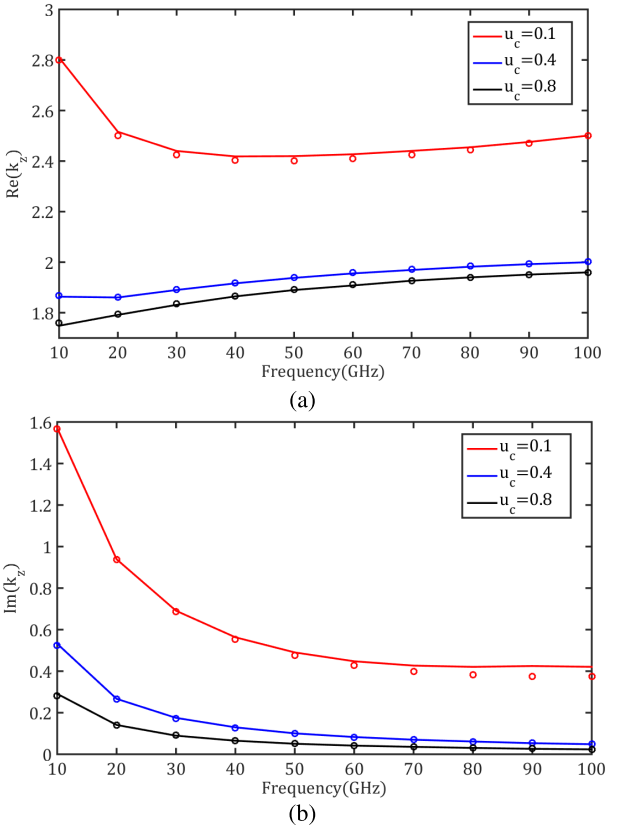

FIGURE 12. The normalized propagation constant of stripline plotted for three chemical potentials and magnetic bias $B_0 = 0.1\ T$: a) real part, b) imaginary part, Solid line: MOL method, Circles: COMSOL Simulation.

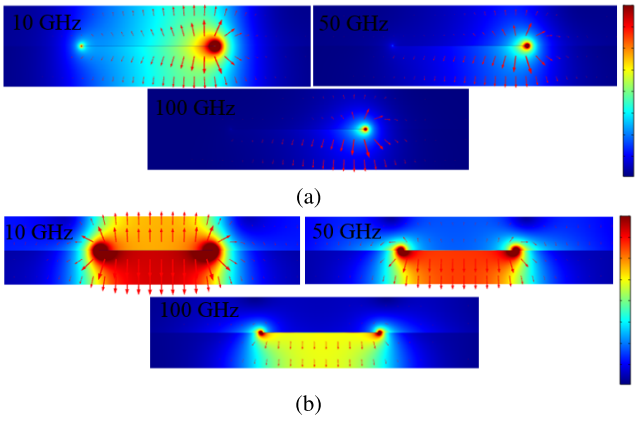

FIGURE 13. Electric field distribution at different frequencies: a) $\mu_c = 0.1$, b) $\mu_c = 0.8$.

C. PARALLEL-PLATE WAVEGUIDE (PPWG)

As the third example of graphene-contained multilayered structures, the results of the analysis of the graphene parallel-plate waveguide using the extended method of lines are presented. The structure of the graphene parallel-plate waveguide is shown in Fig. 14.

The widths of the graphene strips are $w = 1mm$. The analysis of this structure is performed for two values of

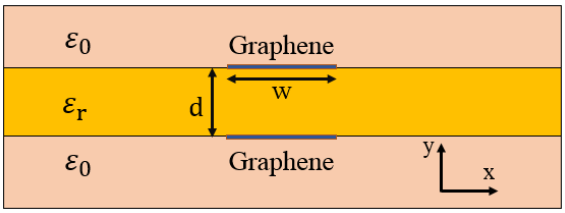

FIGURE 14. Analyzed graphene-based parallel-plate waveguide.

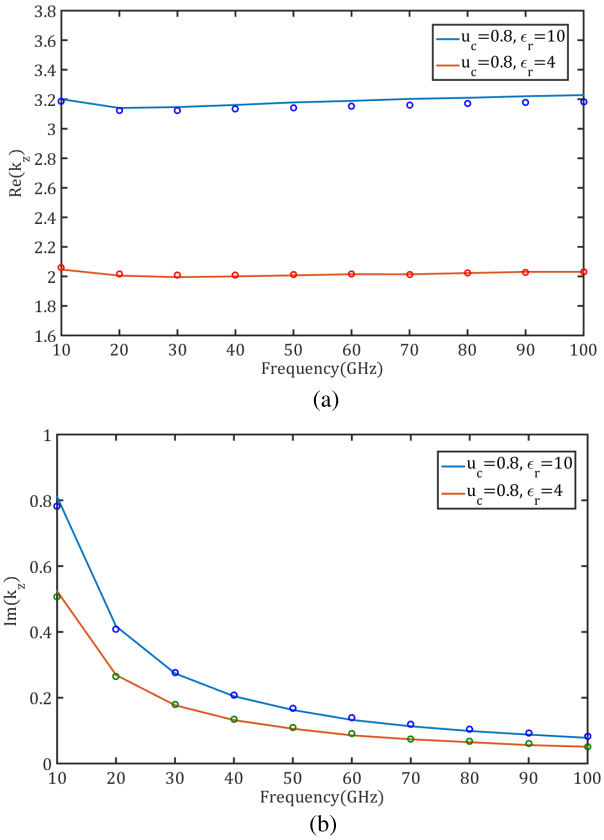

FIGURE 15. The normalized propagation constant for the parallel-plate waveguide plotted for two different permittivities. The magnetic bias is $B_0 = 0.1T$. a) real part, b) imaginary part, Solid line: MOL method, Circles: COMSOL Simulation.

the substrate dielectric permittivity $\varepsilon_r = 4$ and $\varepsilon_r = 10$. The distance between the two graphene strips, and also the graphene magnetic bias are considered $d = 0.2$mm and $B_0 = 0.1T$, respectively. The propagation constant of the parallel-plate waveguide with the above-mentioned characteristics is obtained using MOL method and is compared with COMSOL software simulations. Fig. 15 plots the real and imaginary parts of the propagation constant with respect to the frequency for the chemical potential $\mu_c = 0.8ev$ and for two different values of the substrate dielectric permittivity.

The distributions of the electric field in the graphene parallel-plate waveguide structure at different frequencies for two different dielectric permittivities are shown in Fig. 16.

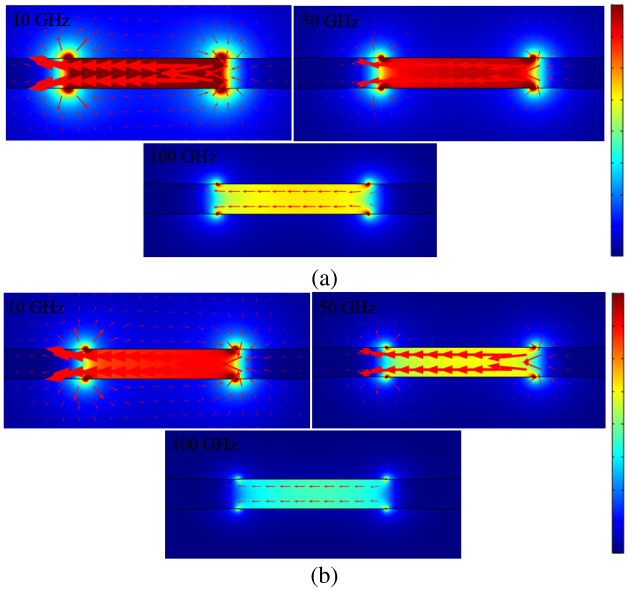

FIGURE 16. Electric field distribution for different frequencies: a) $\varepsilon_r = 4$, b) $\varepsilon_r = 10$.

V. CONCLUSIONS

In this paper, the analysis of the graphene-contained multilayered two-dimensional structures using the extended method of lines is proposed. Multilayered planar waveguides and two-dimensional waveguides in different coordinate systems are examples of such structures which can all be analyzed using the proposed method. In this paper, a generic two-dimensional multilayered structure is considered for the analysis purposes. The graphene plate placed between the layers may cover the interface of the two layers totally or partially, both of which can be analyzed using the proposed method. In the analysis, the graphene conductivity is considered as a tensor. Impedance and admittance transformation formulas at the interface between each two graphene-contained layers are presented. In order to calculate the propagation constant of the structure, the characteristic equation of the graphene-contained multilayered structure is obtained by matching the fields at the interfaces. Using the proposed method, all graphene-contained multilayered structures including waveguide structures, absorbers, and radiators can be analyzed. In the present paper, three waveguide structure test cases including graphene microstrip line, graphene stripline, and graphene parallel-plate waveguide are analyzed using the extended method of lines. To verify of the results, all the aforesaid structures are simulated using COMSOL software. Furthermore, the graphene microstrip line is analyzed using the SDM method. The results are in good agreement. By varying the graphene parameters such as chemical potential, the controllable characteristics of the multilayered structure (here the propagation constant of the analyzed transmission lines) are investigated. The controllability of graphene sheet has many applications in tunable microwave devices. The proposed method can be used and implemented in various kinds of multilayered structures.

REFERENCES

[1] S. He and T. Chen, "Broadband THz absorbers with graphene-based anisotropic metamaterial films," *IEEE Trans. THz Sci. Technol.*, vol. 3, no. 6, pp. 757–763, Nov. 2013.

[2] H. Nasari and M. S. Abrishamian, "Electrically tunable graded index planar lens based on graphene," *J. Appl. Phys.*, vol. 116, no. 8, p. 083106, Aug. 2014.

[3] D. L. Sounas and C. Caloz, "Graphene for highly tunable non-reciprocal electromagnetic devices," in *Proc. IEEE Antennas Propag. Soc. Int. Symp. (APSURSI)*, Jul. 2012, pp. 1–2.

[4] D. L. Sounas and C. Caloz, "Electromagnetic nonreciprocity and gyrotropy of graphene," *Appl. Phys. Lett.*, vol. 98, no. 2, p. 021911, Jan. 2011.

[5] A. Y. Nikitin, F. Guinea, F. J. García-Vidal, and L. Martín-Moreno, "Edge and waveguide terahertz surface plasmon modes in graphene microribbons," *Phys. Rev. B, Condens. Matter*, vol. 84, no. 16, p. 161407, 2011.

[6] D. L. Sounas and C. Caloz, "Edge surface modes in magnetically biased chemically doped graphene strips," *Appl. Phys. Lett.*, vol. 99, no. 23, p. 231902, 2011.

[7] G. W. Hanson, A. B. Yakovlev, and A. Mafi, "Excitation of discrete and continuous spectrum for a surface conductivity model of graphene," *J. Appl. Phys.*, vol. 110, no. 11, p. 114305, 2011.

[8] N. Chamanara, D. Sounas, and C. Caloz, "Non-reciprocal magnetoplasmon graphene coupler," *Opt. Exp.*, vol. 21, no. 9, pp. 11248–11256, May 2013.

[9] D. L. Sounas and C. Caloz, "Gyrotropy and nonreciprocity of graphene for microwave applications," *IEEE Trans. Microw. Theory Techn.*, vol. 60, no. 4, pp. 901–914, Apr. 2012.

[10] H. H. Ardakani, Z. G. Kashani, M. K. Amirkalaee, and J. Rashed-Mohassel, "Fourier transform analysis of graphene-based multilayer structures," *IET Microw., Antennas Propag.*, vol. 7, no. 13, pp. 1084–1091, Oct. 2013.

[11] A. G. D'Aloia, M. D'Amore, and M. S. Sarto, "Terahertz shielding effectiveness of graphene-based multilayer screens controlled by electric field bias in a reverberating environment," *IEEE Trans. THz Sci. Technol.*, vol. 5, no. 4, pp. 628–636, Jul. 2015.

[12] G. W. Hanson, "Dyadic green's functions for an anisotropic, non-local model of biased graphene," *IEEE Trans. Antennas Propag.*, vol. 56, no. 3, pp. 747–757, Mar. 2008.

[13] D. L. Sounas and C. Caloz, "Graphene-based non-reciprocal spatial isolator," in *Proc. IEEE Int. Symp. Antennas Propag. (APSURSI)*, Jul. 2011, pp. 1597–1600.

[14] G. W. Hanson, "Quasi-transverse electromagnetic modes supported by a graphene parallel-plate waveguide," *J. Appl. Phys.*, vol. 104, no. 8, p. 084314, Oct. 2008.

[15] A. Madani, S. Zhong, H. Tajalli, S. Roshan Entezar, A. Namdar, and Y. Ma, "Tunable metamaterials made of graphene-liquid crystal multilayers," *Prog. Electromagn. Res.*, vol. 143, pp. 545–558, 2013.

[16] N. Chamanara, D. Sounas, T. Szkopek, and C. Caloz, "Optically transparent and flexible graphene reciprocal and nonreciprocal microwave planar components," *IEEE Microw. Wireless Compon. Lett.*, vol. 22, no. 7, pp. 360–362, Jul. 2012.

[17] U. Schulz and R. Pregla, "A new technique for the analysis of the dispersion characteristics of planar waveguides and its application to microstrips with tuning septums," *Radio Sci.*, vol. 16, no. 6, pp. 1173–1178, 1981.

[18] F. J. Schmuckle and R. Pregla, "The method of lines for the analysis of planar waveguides with finite metallization thickness," *IEEE Trans. Microw. Theory Techn.*, vol. 39, no. 1, pp. 107–111, Jan. 1991.

[19] W. Pascher and R. Pregla, "Analysis of rectangular waveguide junctions by the method of lines," *IEEE Trans. Microw. Theory Techn.*, vol. 43, no. 12, pp. 2649–2653, Dec. 1995.

[20] R. Pregla, "Efficient and accurate modeling of planar anisotropic microwave structures by the method of lines," *IEEE Trans. Microw. Theory Techn.*, vol. 50, no. 6, pp. 1469–1479, Jun. 2002.

[21] W. Pascher and R. Pregla, "Full wave analysis of complex planar microwave structures," *Radio Sci.*, vol. 22, no. 6, pp. 999–1002, Nov. 1987.

[22] S. B. Worm and R. Pregla, "Hybrid-mode analysis of arbitrarily shaped planar microwave structures by the method of lines," *IEEE Trans. Microw. Theory Techn.*, vol. 32, no. 2, pp. 191–196, Feb. 1984.

[23] T. Itoh, *Numerical Techniques for Microwave and Millimeter-Wave Passive Structures*. Hoboken, NJ, USA: Wiley, 1989.

[24] H. H. Ardakani, A. Mehrdadian, and K. Forooraghi, "Analysis of graphene-based microstrip structures," *IEEE Access*, vol. 5, pp. 20887–20897, 2017.

ALI MEHRDADIAN was born in Sabzevar, Iran, in 1987. He received the B.S. degree in electrical engineering from the K. N. Toosi University of Technology, Tehran, in 2009, and the M.Sc. degree in communication engineering from Tarbiat Modares University, Tehran, in 2012, where he is currently pursuing the Ph.D. degree. His main interests include UWB antennas, antenna arrays, filters, and numerical methods in electromagnetics.

HOSSEIN HATEFI ARDAKANI was born in Ardakan, Iran, in 1985. He received the B.S. degree in electrical engineering from the Isfahan University of Technology, Isfahan, Iran, in 2007, and the M.S. degree in electrical engineering from the University of Tehran, Tehran, Iran, in 2010, with a focus on the analysis of planar transmission lines on bianisotropic substrates. He is currently pursuing the Ph.D. degree in applied electromagnetics with Tarbiat Modares University, Tehran. His main research interests include electromagnetics theory, analytical/numerical methods in electromagnetics and metamaterials.

KEYVAN FOROORAGHI received the M.Sc. degree in electrical engineering and the licentiate of technology degree from the Chalmers University of Technology, Gothenburg, Sweden, and the Ph.D. degree in electrical engineering from the Chalmers University of Technology in 1991. He was a Researcher with the Chalmers University of Technology from 1991 to 1992. In 1992, he joined the Department of Computer and Electrical Engineering, Tarbiat Modares University, where he is currently a Full Professor with the Communication Group. His research interests include electromagnetic theory and computational electromagnetic and antenna theory.